Numerical Modelling of Fully Grouted Rock Bolts using a 2D Finite Element Method

Ya Su
College of Civil Engineering – Hunan University, Changsha, Hunan, China & Department of Geological Sciences and Geological Engineering – Queen's University, Kingston, Ontario, Canada

Nicholas Vlachopoulos
GeoEngineering Centre Queen's-RMC, Department of Civil Engineering – Royal Military College of Canada, Kingston, Ontario, Canada

ABSTRACT
Rock bolts are one of the primary underground support systems utilized to stabilize the rock mass surrounding the opening of an excavation by transferring the load from the surrounding rock to the more stable rock mass further from the excavation. Modelling fully grouted rock bolts has been the focus of many researchers due to the difficulties associated with capturing the interaction mechanism(s) concerning the interface between the rebar and the grout as well as the grout and the rock at the micro-scale. In this paper, two-dimensional (2D) numerical simulations have been conducted in order to model the behaviour of fully grouted rock bolts (FGRBs) during axial pullout tests. Joint parameters of the rebar-grout interface (i.e. shear stiffness, normal stiffness and cohesion) are investigated as well as grout parameters (i.e. Poisson's ratio and Young's modulus) in terms of the influence on the rock bolt behaviour. The results indicate that the Young's modulus of the grout and joint shear stiffness have significant influences on the overall behaviour and performance of the FGRB system. On the basis of these results, the upper and lower limit of strain distribution along with the rock bolt is determined. These results are also compared to the nominally identical axial pullout tests of rock bolts that have been conducted in the laboratory as part of the physical testing components of the overall research program.

RÉSUMÉ
Les boulons d'ancrage sont l'un des principaux systèmes de souterrain utilisés pour stabiliser la masse rocheuse entourant l'ouverture d'une excavation en transférant la charge de la roche environnante vers la masse rocheuse plus stable plus loin de l'excavation. La modélisation de boulons de roche entièrement jointoyés a été au centre de nombreux chercheurs en raison des difficultés associées à la capture du ou des mécanismes d'interaction concernant l'interface entre les barres d'armature et le coulis ainsi que le coulis et la roche à la micro-échelle. Dans cet article, des simulations numériques bidimensionnelles (2D) ont été menées afin de modéliser le comportement des boulons de roche entièrement injectés (FGRB) lors d'essais de retrait axial. Les paramètres communs de l'interface barres d'armature (c.-à-d. La rigidité au cisaillement, la rigidité et la cohésion normales) sont étudiés ainsi que les paramètres du coulis (c.-à-d. Le coefficient de Poisson et le module d'Young) en termes d'influence sur le comportement du boulon d'ancrage. Les résultats indiquent que le module d'Young du coulis et la rigidité au cisaillement des joints ont une influence significative sur le comportement et les performances globales du système FGRB. Sur la base de ces résultats, la limite supérieure et inférieure de la distribution des déformations avec le boulon d'ancrage a été déterminée. Ces résultats sont également comparés à des essais de retrait axial des boulons d'ancrage nominalement identiques qui ont été menés en laboratoire dans le cadre des éléments d'essai physique du programme de recherche global.

1 INTRODUCTION

Reinforcement systems play a significant role in underground construction projects due to the rising demand for the ability to overcome difficulties encountered due to excavation works in mines, tunnels or other geotechnical engineering operations. Rock bolts have been utilized as part of reinforcing systems in order to stabilize rock mass adjacent to the excavation periphery in underground construction projects such as mining and tunnel engineering excavations dates since the last century. Generally, they reinforce rock masses by restraining the deformation surrounding the excavation boundary (Stillborg 1986). In this manner, the rock masses transmit load experienced by them to the rock bolt (Li and Stillborg 1999; Vlachopoulos et al. 2018,

2020). The load transfer among the rock and the bolt is decisive for the reinforcement effect of the rock bolt. Windsor (1997) states that a rock bolt system consists of four main components, namely, the rock, the reinforcing element, the internal fixture and the external fixture, as presented in Figure 1. The load transfer interactions among the components can also be found in the figure.

In order to effectively increase the efficiency of the load transfer from the rock, multiple devices have been developed as well as modifications to rock bolts. Based on the various mechanical interactions associated with the load transfer, the current, industry standard, rock reinforcement devices are categorized as three fundamental types (Windsor 1997): (1) Continuously Mechanically Coupled (CMC), (2) Continuous Frictionally Coupled (CFC) and, (3) Discretely Mechanically or Frictionally Coupled (DMFC), as illustrated in Figure 2. In CMC bolts, the load is transferred continuously along the length of the bolt through a medium such as grout or resin; In CFC bolts, the load is transmitted constantly along the bolt length through a frictional contact at the bolt/rock interface; while in DMFC bolts, the load is delivered discretely by resin or grout or over a mechanical device, such as anchors, that provides frictional capacity (Bobet and Einstein 2011; He et al. 2015).

Fully grouted rock bolts (FGRBs) belong to the CMC system. Due to ease installation, relative low cost and safety considerations, the FGRBs have been the most widely used for work support purposes within civil and mining engineering works. It can be seen in Figure 1 that the reinforcing element (or composite support system made up of multiple components) refers to the bolt itself for the FGRBs, the internal fixture represents the material such as grout transmitting load between the rock and the bolt, and the external fixture is arranged in order to aid in the load transfer at the excavation periphery, namely, the faceplate assembly. For the FGRBs, the load transfer throughout the system occurs primarily in the shear resistance induced along with the interfaces of different materials (Vlachopoulos et al. 2018). The loading of the FGRBs is also significantly impacted by the system installation orientation compared with the rock mass deformation vector (Mark et al., 2002). These factors can result in the loading conditions of the FGRBs as axial loading or shearing, separately caused by bed dilation/separation or slip along the bedding plane, as shown in Figure 3. This study is only focused on the FGRB behaviour under the axial loading. As there has been a rise in demand for a more geomechanically based understanding of the behaviour and performance of the FGRBs, methods such as field monitoring and testing, laboratory tests, analytical approaches, numerical modelling or a combination have been utilized; These fields / methods are also improving in their own right.

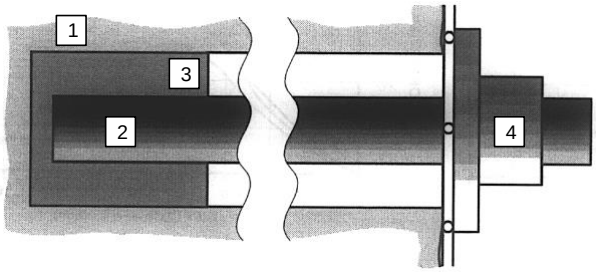

Components	Load Transfer Interactions
1. The Rock	1 - 3; 1 - 4
2. The Reinforcing Element	2 - 3; 2 - 4
3. The Internal Fixture	3 - 4
4. The External Fixture	

Figure 1. Main components of a rock bolt reinforcing system as well as load transfer interactions (modified after Windsor 1997).

2 BACKGROUND

As Freeman (1978) firstly conducted monitoring work on the fully-bonded rock bolts in order to understand the loading process along the embedded bolt length as well as the stress distribution behavior. Since then, numerous studies aiming at investigating on the load transfer interactions within the rock bolt system have been carried out. Field monitoring and testing (Bigby 2004; Choquet and Miller 1988; Hyett et al. 1992; Rong et al. 2004; Signer 1990; Sun 1984), laboratory tests (Azziz and Webb 2003; Benmokrane et al. 1995; Hagan 2004; Hyett et al. 1995; Moosavi et al. 2005; Vlachopoulos and Diederichs 2014; Vlachopoulos and Forbes 2018; Vlachopoulos et al. 2014a, 2014b, 2017, 2018, 2020) and analytical approaches (Farmer 1975; Indraratna and Kaiser 1990; Kaiser and Yacizi 1992; Li and Stillborg 1999; Ren et al. 2009) have been developed over the years. Considering the cost of field monitoring and laboratory tests as well as the limitation of analytical approaches, numerical modelling can provide an alternative way to investigate the rock bolt loading behaviour.

There have been a variety of different numerical software packages utilized as numerical analysis tools. In terms of the numerical modelling of the FGRB, finite element methods, such as ANSYS (Ghadimi et al. 2015; Jalalifar and Aziz 2012), RS2 (Cruz 2017), and finite difference methods, such as FLAC 2D and 3D (Ma et al. 2016; Nemcik et al. 2014) have been investigated. In order to model the axial loading condition conducted as part of this study, the finite element software RS2 (Rocscience Inc. 2016) was used. The rational and background can be seen within Cruz (2017) and Vlachopoulos et al. (2020).

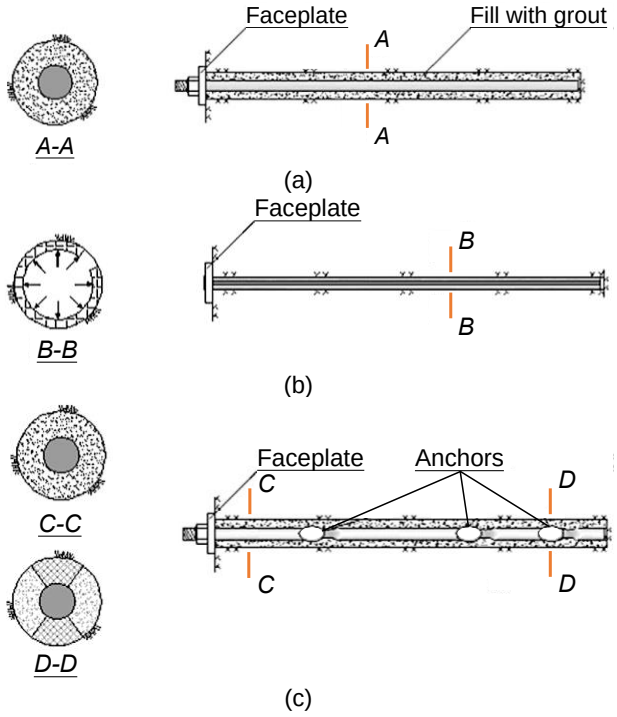

Figure 2. Three fundamental rock bolt types: (a) CMC rock bolts (i.e. fully grouted rebar), (b) CFC rock bolts (i.e. split set) and (c) DFMC rock bolts (i.e. the D-bolt) (modified after Nie et al. 2019; Windsor and Thompson 1993).

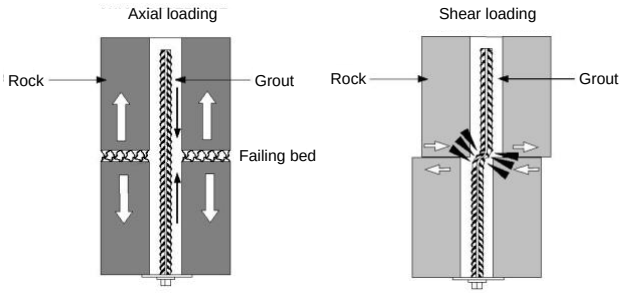

Figure 3. Typical loading categories of FGRBs (modified after Mark et al. 2002).

RS2 (RocScience Inc. 2016) is a two-dimensional (2D) finite element program designed for engineering projects including underground rock excavation and design. A wide range of support modelling options and failure criteria are available in RS2. Different types of rock bolts can be modelled, such as end anchored rock bolts, fully bonded rock bolts and swellex / split sets rock bolts. RS2 has the capability to model the FGRB as a combination of different bolt elements. As can be seen in Figure 4, the bolt itself is consisted of numerous elements, on the basis of the specific condition of the finite element mesh. Each bolt element acts independently and has an indirect effect on other bolt elements and is also influenced by the ground elements.

As part of this analysis, it was considered that failure has occurred in the FGRB model once the axial loading over the bolt element exceeds the axial loading capacity of the bolt. In addition, it is assumed that before failure the bolt is fully bonded to the rock. Accordingly, the interface parameters such as strength and stiffness between the grout and the rock are not taken into account as well as between the bolt and the grout. This is a limitation of the software. However, such an arrangement does allow to initially estimate the supporting pattern of a rock bolt. As a result, in this study the FGRB was simulated as a combination of independent elements and individual materials, while taking into account the joint between the bolt and the grout.

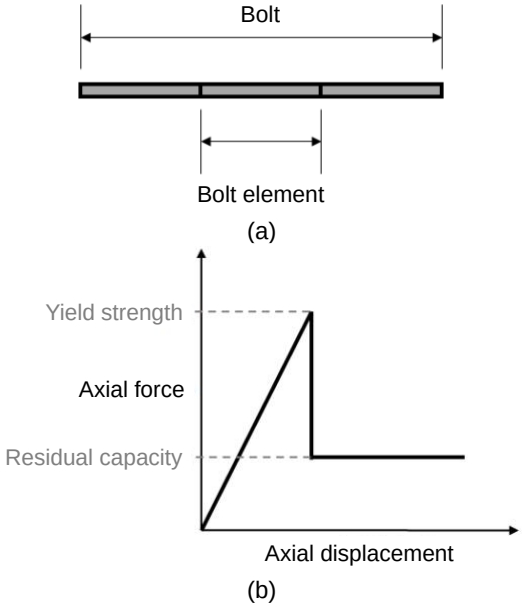

Figure 4. The FGRB elements in RS2. (a) Bolt model, (b) FGRB Failure criteria (modified after RocScience Inc. 2016).

3 FINITE ELEMENT MODELLING

3.1 Laboratory Axial Pullout Test

In order to study the mechanistic response of a FGRB, axial pullout tests were carried out within the structure laboratory at the Royal Military College of Canada (RMC). These tests were performed using a cement-based FGRB. With reference to Figure 1, the components of the FGRB specimen in this numerical study are successively, the pipe (simulated rock), rebar (the rock bolt), cement (the grout) and the faceplate assembly. The strains along the rebar were measured using a Fiber Optic Sensors (FOS) developed at RMC as discussed by Vlachopoulos et al. (2018). The configuration of the laboratory pullout test is shown in Figure 5.

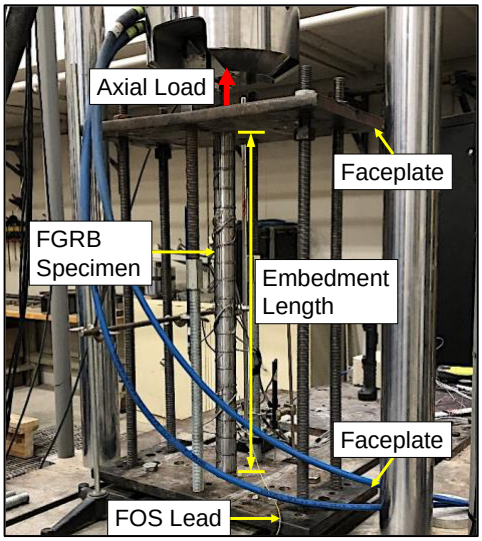

Figure 5. Laboratory pullout test configuration

3.2 Model Geometry, Loading and Boundary Conditions

Due to the symmetry of the FGRB specimen, an axisymmetric RS2 finite element model was developed and built as shown in Figure 6(a). This was selected over plain strain analysis. It is comprised of the main components, i.e. rebar, grout and pipe. The dimensions of the three materials can be found in Table 1. The bolt-grout interface was modelled explicitly by defining a joint boundary between the two materials, while the grout-pipe interface was modelled by choosing a material boundary. Different models were created with various embedment lengths as obtained from the laboratory testing component of the overall research program. Figure 6(b) illustrates the axial pullout load over the bolt and the restraint conditions. The mesh was discretized into a graded mesh. The axial pullout force increases progressively in the modelling process up to the maximum value of 120 kN. In addition, a constant field stress of 10 MPa was applied across the model for the purpose of simulating the confinement provided during the laboratory test. Moreover, location distance x was set as $x = 0$ with respect to the fixed end of the embedment that is near the applied axial loading location, as shown in Figure 6. The distance increases from the near end of the embedment length to the far end. The strains along the embedment length, i.e. from $x = 0$, were computed and output.

Table 1. Numerical model dimensions

Material properties	Rebar	Grout	Pipe
Diameter D (mm)	19.05	-	48.30
Thickness h (mm)	-	10.93	7.40

3.3 Material Model and Properties

The material parameters selected in the numerical model can be found in Table 2. The model materials were modelled using the Mohr-Coulomb failure criterion. This requires cohesion, friction angle and tensile strength of the materials measured or calculated from the laboratory tests. Additionally, all the model materials were simulated to be isotropic and elastic. As for the material boundaries, the joint parameters obtained from the laboratory testing results are listed in Table 3 (Cruz 2017) since the bolt-grout interface was modelled as a joint. Open condition of the joint ends was chosen, which indicates the two nodes representing the ends of the joint boundary can move independently. This is in accordance with the laboratory testing conditions.

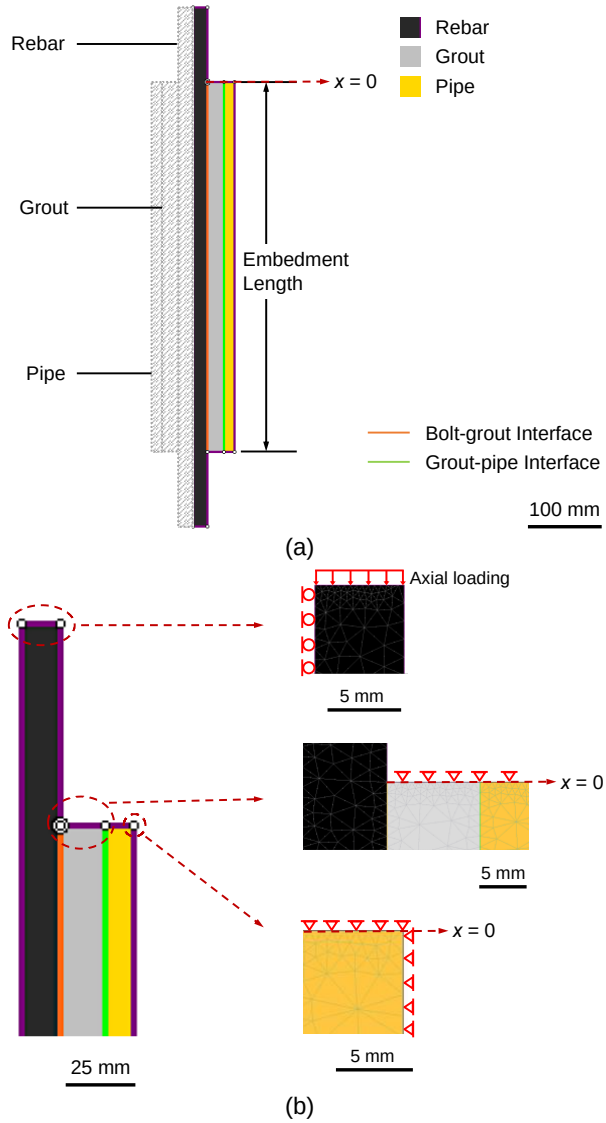

Figure 6. 2D finite element model configuration, axial loading and boundary conditions. (a) Symmetric model configuration; (b) Loading and boundary conditions.

Table 2. Numerical model material properties

Material properties	Rebar	Grout	Pipe
Unit weight γ (MN/m3)	0.078	0.023	0.078
Cohesion c (MPa)	310	0.4	310
Poisson's ratio ν	0.30	0.14	0.30
Young's modulus E (MPa)	200000	8190	200000
Friction angle ϕ (°)	0	35	0
Tensile strength (MPa)	620	1.8	413

Table 3. Bolt-grout interface joint properties (modified after Cruz 2017)

Joint properties	Value
Normal stiffness (MPa/m)	120000
Shear stiffness (MPa/m)	100000
Cohesion c (MPa)	Varies
Residual Cohesion c_R (MPa)	0
Friction angle ϕ (°)	0
Residual friction angle ϕ_R (°)	50

4 SELECTED MODELLING RESULTS

In order to understand the sensitivity of the mechanical response of the FGRB system that was examined, parametric analyses were conducted with selected parameters of the bolt-grout joint interface, i.e. normal stiffness, shear stiffness, and cohesion, and of the grout material, i.e. Young's modulus and Poisson's ratio. Four values (levels) of a particular parameter were chosen in each of the parametric analysis (Table 4) while other parameters were taken as constants. The strain along the bolt-grout interface and the grout-pipe interface were respectively plotted versus the distance of locations along the same interface. As mentioned in Section 3.2, the distance of the fixed end that is near the loading location is zero. Additionally, results of the numerical simulation were obtained and compared to those recorded in the nominally identical laboratory tests.

Table 4. Levels of parameters used in parametric analyses

Selected parameters	Level 1	Level 2	Level 3	Level 4
Bolt-grout joint interface				
Normal stiffness (MPa/m)	0	50000	100000	500000
Shear stiffness (MPa/m)	1000	10000	100000	500000
Cohesion (MPa)	10	20	30	300
Grout material				
Young's modulus (MPa)	10000	30000	50000	80000
Poisson's ratio	0.1	0.2	0.3	0.4

4.1 Effect of Bolt-grout Joint Parameters

Figure 7 shows the effect of the change in joint normal stiffness (i.e. 0, 50000, 100000 and 500000 MPa/m) on the strain at the two material boundaries. Generally, the strain along the grout-pipe interface is smaller than that for the bolt-grout interface. Different from the decreasing strain tendency in Figure 7(a), the strain illustrated in Figure 7(b) reduces once the distance reaches 0.028 m, after a rise of the strain value. This is due to limited restrains and open joint selection for the near end of the bolt-grout interface in the numerical model while restraining set for the same location at the grout-pipe interface. It indicates in the figures that the strain curves of the both interfaces have negligible change with varying joint normal stiffness.

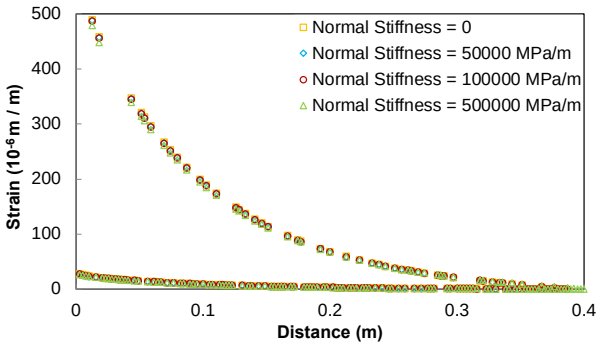

(a)

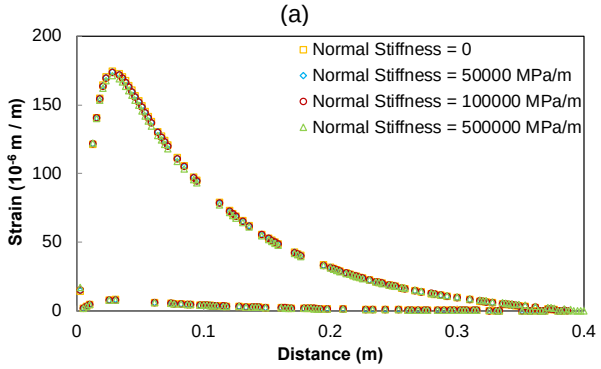

(b)

Figure 7. Evolution of strain with varying joint normal stiffness values. (a) Strain evolution along bolt-grout interface; (b) Strain evolution along grout-pipe interface.

Unlike the previous parameter, joint shear stiffness has a direct effect on the bolt mechanical behaviour as illustrated in Figure 8. When joint shear stiffness is chosen as 1000 MPa/m, the strain is relatively small and almost unchanging along the whole bolt. During the increase in joint shear stiffness, the tendency of strain changes obviously as well as the strain magnitude.

When joint shear stiffness reaches 500000 MPa/m, the strain at the maximum point along the bolt-grout interface is rising to more than ten times and over five times with respect to the grout-pipe interface. Besides, the slope of the strain curve is clearly becoming greater as the value of this parameter rises.

Figure 9 presents the effect of joint cohesion on the strain. Analyses were conducted with joint cohesion value at 10, 20, 30 and 300. Similar to Figure 7, the resulting magnitude and tendency of the strain nearly stay unchanged for both the bolt-grout interface and the grout-pipe interface as the cohesion varies. This means joint cohesion does not have a significant influence on the strain numerically.

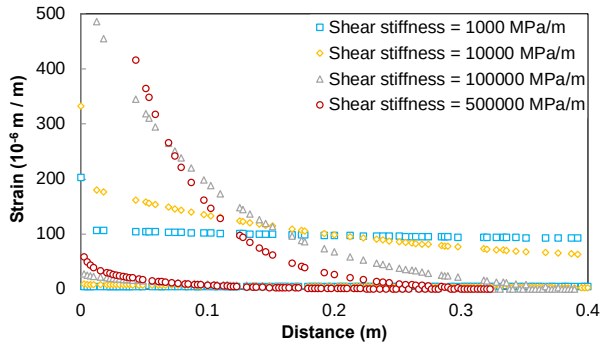

(a)

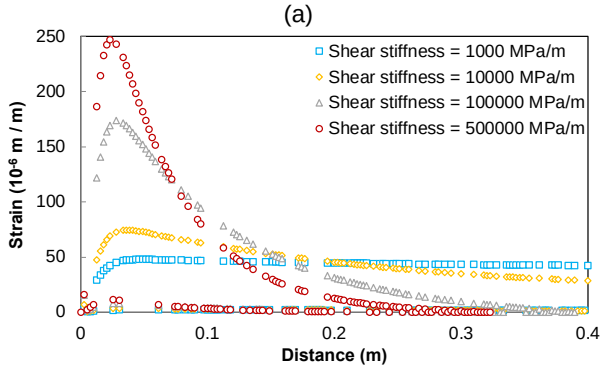

(b)

Figure 8. Evolution of strain with varying joint shear stiffness values. (a) Strain evolution along bolt-grout interface; (b) Strain evolution along grout-pipe interface.

4.2 Effect of Grout Parameters

Figure 10 demonstrates the strain influenced by the variation of grout Young's modulus at 10000, 30000, 50000 and 80000 MPa, respectively. For a location near the end of the bolt, the strain is clearly decreasing at both interfaces as the Young's modulus becomes larger. The maximum stain value reduces by approximately 86% for the bolt-grout interface when Young's modulus increases from 10000 to 80000 MPa, while this percentage is about 90% for the grout-pipe interface. However, this phenomenon diminishes when the distance rises, meaning that the strain sensitivity to this parameter diminishes with the location – i.e. farther from the end of the bolt. Additionally, the strain curves have similar tendencies for each interface, and the tendency gradually becomes mild with increasing grout Young's modulus.

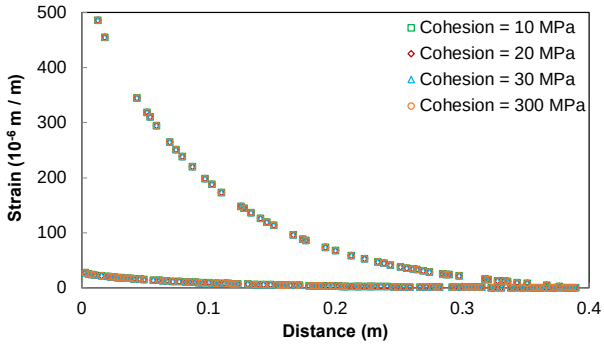

(a)

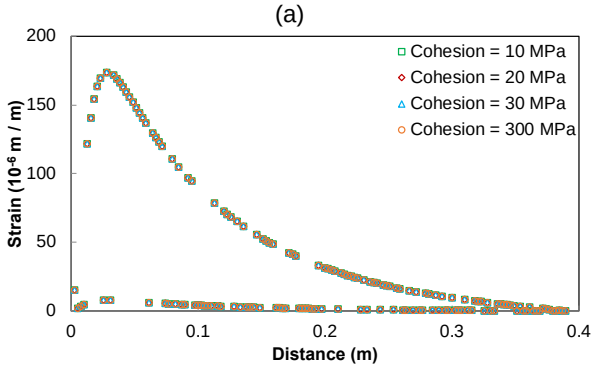

(b)

Figure 9. Evolution of strain with varying joint cohesion values. (a) Strain evolution along bolt-grout interface; (b) Strain evolution along grout-pipe interface.

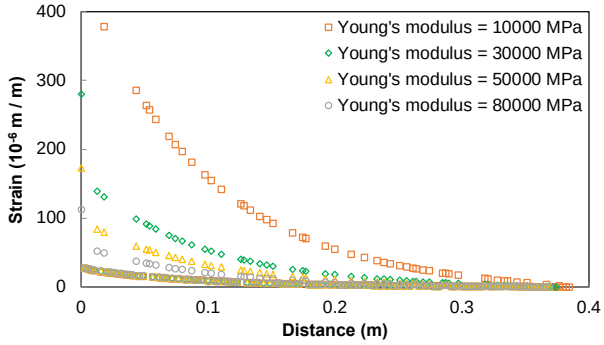

(a)

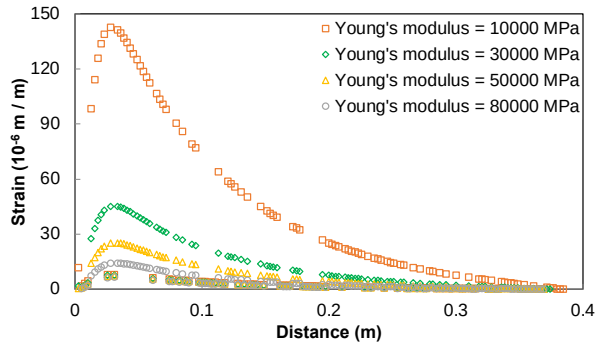

(b)

Figure 10. Evolution of strain with varying grout Young's modulus values. (a) Strain evolution along bolt-grout interface; (b) Strain evolution along grout-pipe interface.

Figure 11 presents the impact of grout Poisson's ratio on the strain. Four levels of the Poisson's ratio were selected, i.e. 0.1, 0.2, 0.3 and 0.4. It can be seen within the figure that the strain values become slightly larger as Poisson's ratio increases from 0.1 to 0.4, wherein the maximum strain at the bolt-grout interface and the grout-pipe interface rises by 24% and 18%, respectively. Generally, the strain curves for each interface are almost parallel to each other, indicating the strain changing tendency of the curves are highly similar. Accordingly, the strain is slightly sensitive to the grout's Poisson's ratio.

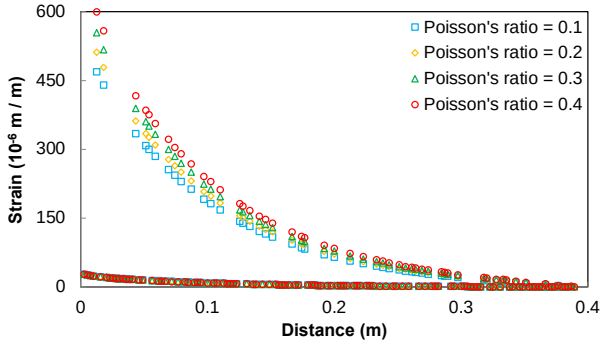

(a)

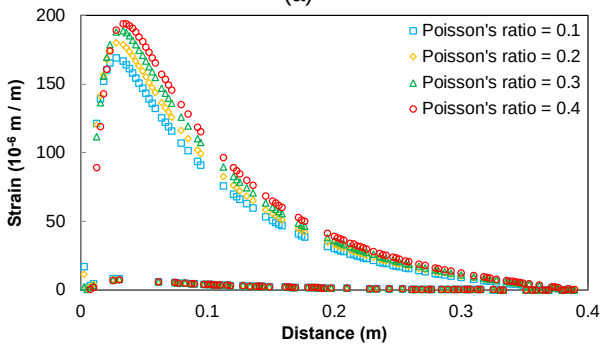

(b)

Figure 11. Evolution of strain with varying grout Poisson's ratio values. (a) Strain evolution along bolt-grout interface; (b) Strain evolution along grout-pipe interface.

4.3 Strain Analysis

The numerical models were analyzed with respect to the strain along rebar for different bolt embedment lengths of 0.25m, 0.50m and 0.75m, respectively, were considered. Figures 12 to 14 illustrates strain comparisons between numerical modelling and laboratory tests (O'Connor et al. 2019) under an axial loading condition of 20kN.

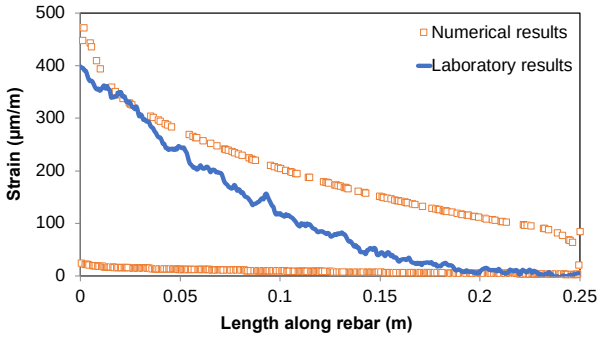

Figure 12. Result comparison between numerical modelling and laboratory tests in terms of 0.25m embedment length.

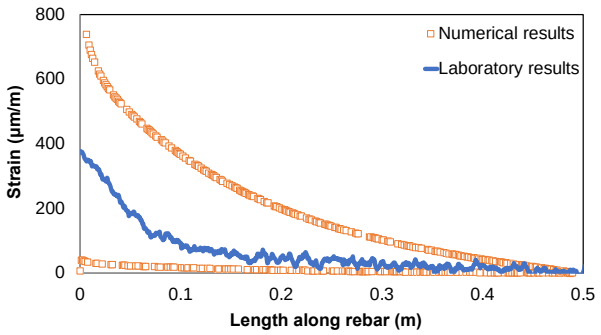

Figure 13. Result comparison between numerical modelling and laboratory tests in terms of 0.50m embedment length.

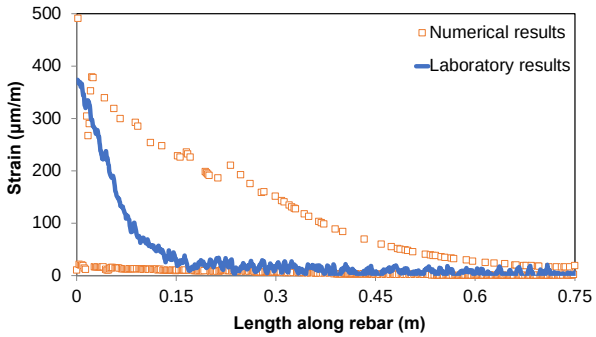

Figure 14. Result comparison between numerical modelling and laboratory tests in terms of 0.75m embedment length.

It can be seen in the figures above that the numerical simulations predict a value interval consisting of two curves while most of the laboratory results are within the value interval given by the numerical results. Moreover, the strain distribution tendency of the numerical results is in accordance with that of the laboratory results. As such, the two curves obtained from the numerical simulation can be taken as the upper limit and lower limit of the strain of FGRB for such axial pullout tests.

On the basis of the previous sections, the joint shear stiffness G_j and the grout Young's modulus E_g play significant roles in terms of the sensitivity analyses of strain ε along the bolt. From this perspective, ε can be determined as a function of G_j and E_g, expressed as

$$\varepsilon = f(G_j, E_g) \quad (1)$$

Using Equation 1, the upper and lower limits of ε can be determined. It should be noted that G_j is a fictitious input parameter for numerical modelling purposes, and it is an issue to address the correlation between G_j and the parameters that can be measured and calculated in the site or laboratory.

5 CONCLUSION

This paper investigated the mechanical response of FGRB under an axial loading condition using two-dimensional numerical modelling in order to establish its relevance to such works with respect to effectively determining the performance and behaviour of FGRBs. As such, a numerical model was created to simulate an identical FGRB specimen that were used in multiple laboratory pullout tests conducted in the Royal Military College of Canada. Numerical simulations were carried out to simulate the laboratory pullout testing process. The numerical results were compared to those obtained in the laboratory tests, indicating that the tendencies of the numerical results are in accordance with the laboratory results.

Parametric analyses were also conducted in order to determine the sensitivity of the strain along the two material interfaces of the FGRB, in which selected joint properties and grout parameters are involved. It is concluded the shear stiffness of the bolt-grout joint interface and the Young's Modulus of the grout material have dominant effects on the result. As such, the strain can be taken as a function of these two crucial parameters, as well as the corresponding upper and lower strain limits.

This study provides a better understanding on the FGRB behaviour in the pullout test. Further research will focus on determining a reasonable relationship between the strain along the bolt and the two critical parameters, especially the joint shear stiffness, by utilizing numerical modelling, an observational approach as well as other techniques which can improve the numerical technique presented herein for FGRB modelling. Such improvements to calibrated models of this nature will aid design engineers with their preliminary support designs.

ACKNOWLEDGEMENTS

The authors would like to thank the Royal Military College (RMC), the RMC Green Team, the Department of National Defence, Canada, the Natural Sciences and Engineering Research Council (NSERC) and the China Scholarship Council (CSC) for supporting this research.

REFERENCES

ANSYS finite element software. *ANSYS*. Inc., Canonsburg, PA, USA.

Azziz, N. and Webb, B. 2003. Study of load transfer capacity of bolts using short encapsulation push tests. *Coal Operators' Conference*, University of Wollongong, Australia.

Benmokrane, B., Chennouf, A. and Mitri, H.S. 1995. Laboratory Evaluation of Cement-Based Grouts and Grouted Rock Anchors. *International Journal of Rock Mechanics and Mining Sciences*, 32: 633-642.

Bigby, D. 2004. *Coal mine roadway support system handbook,* United Kingdom.

Bobet, A. and Einstein, H.H. 2011. Tunnel reinforcement with rockbolts. *Tunnelling and Underground Space Technology*, 26(1): 100-123.

Choquet, P. and Miller, F. 1988. Development and field testing of a tension measuring gauge for cable bolts used as ground support. *CIM Bulletin*, 81(915): 53-59.

Cruz, D.F. 2017. *The geomechanical response of axially loaded fully grouted rock bolts utilizing fibre optics technology*. Master of science thesis, Royal Military College of Canada, Kingston, ON, Canada.

Farmer, I.W. 1975. Stress Distribution along a Resin Grouted Rock Anchor. *International Journal of Rock Mechanics and Mining Sciences*, 12: 347-351.

Freeman, T.J. 1978. The behaviour of fully-bonded rock bolts in the Kielder experimental tunnel. *Tunnels and Tunnelling*, 37-40.

Fuller, P.G., Hume, B.G. and Hume, R.G. 1996. Bolt load simulation and its practical application. *Rock mechanics*, eds. Aubertin, Rotterdam, Netherlands.

Ghadimi, M., Shahriar, K. and Jalalifar, H. 2015. Optimization of the fully grouted rock bolts for load transfer enhancement. *International Journal of Mining Science and Technology*, 25(5): 707-712.

Hagan, P.C. 2004. Variation in load transfer of a fully encapsulated rockbolt. *In Proceedings 23rd International Conference on Ground Control in Mining*. Morgantown, Australia.

He, L., An, X.M. and Zhao, Z.Y. 2015. Fully Grouted Rock Bolts: An Analytical Investigation. *Rock Mechanics and Rock Engineering*, 48: 1181–1196.

Hyett, A.J., Bawden, W.F., Macsporran, G.R. and Moosavi. M. 1995. A Constitutive Law for Bond Failure of Fully-grouted Cable Bolts Using a Modified Hoek Cell. *International Journal of Rock Mechanics and Mining Sciences*, 32: 11-36.

Hyett, A.J., Bawden, W.F. and Reichert, R.D. 1992. The Effect of Rock Mass Confinement on the Bond Strength of Fully Grouted Cable Bolts. *International Journal of Rock Mechanics and Mining Sciences*, 29: 503-524.

Indraratna, B. and Kaiser, P.K. 1990. Analytical model for the design of grouted rock bolt. *International Journal for Numerical and Analytical Methods in Geomechanics*, 227–51.

Ivanović, A. and Neilson, R.D. 2009. Modelling of debonding along the fixed anchor length. *International Journal of Rock Mechanics and Mining Sciences*, 46: 699-707.

Jalalifar, H. and Aziz, N. 2012. Numerical simulation of fully grouted rock bolts. *In M. Andriychuk (Eds.), Numerical Simulation: From Theory to Industry*, USA.

Kaiser, P.K. and Yacizi, S. 1992. Bond Strength of Grouted Cable Bolts. *International Journal of Rock Mechanics and Mining Sciences*, 29: 279-292.

Li, C. and Stillborg, B. 1999. Analytical models for rock bolts, *International Journal of Rock Mechanics and Mining Sciences*, 36(8): 1013-1029.

Ma, S., Zhao, Z., Nie, W. and Gui, Y. 2016. A numerical model of fully grouted bolts considering the tri-linear shear bond–slip model. *Tunnelling and Underground Space Technology*, 54: 73-80.

Mark, C., Compton, C.S., Oyler, D.C. and Dolinar, D.R. 2002. Anchorage pull testing for fully grouted roof bolts. *In Proceedings of the 21st International Conference on Ground Control in Mining*, West Virginia University, Morgantown, WV, USA, 105-113.

Moosavi, M., Jafari, A. and Khosravi, A. 2005. Bond of cement grouted reinforcing bars under constant radial pressure. *Cement and Concrete Composites*, 27: 103-109.

Nemcik, J., Ma, S., Aziz, N., Ren, T. and Geng, X. 2014. Numerical modelling of failure propagation in fully grouted rock bolts subjected to tensile load. *International Journal of Rock Mechanics and Mining Sciences*, 71: 293-300.

Nie, W., Zhao, Z.Y., Guo, W., Shang, J. and Wu, C. 2019. Bond-slip modeling of a CMC rockbolt element using 2D-DDA method, *Tunnelling and Underground Space Technology*, 85: 340-353.

O'Connor, T., Forbes, B., Vlachopoulos, N. and Diederichs, M. 2019. *In Proceedings of the 72nd Canadian Geotechnical Conference*, St. John's, Newfoundland and Labrador, Canada.

Ren, F.F., Yang, Z.J., Chen, J.F. and Chen, W.W. 2009. An analytical analysis of the full range behaviour of grouted rockbolts based on a tri-linear bond-slip model. *Construction and Building Materials*, 24: 361-370.

RocScience Inc. 2016. Bolt Formulation. *Phase2 Theory*, Retrieved from RocScience.

Rong, G., Zhu, H.C. and Zhou, C.B. 2004. Testing study on working mechanism of fully grouted bolts of thread steel and smooth steel. *Chinese Journal of Rock Mechanical Engineering*, 23(3): 469-475.

Signer, S.P. 1990. *Field verification of load-transfer mechanics of fully grouted roof bolts*, United States.

Stillborg, E.B. 1986. *Professional users handbook for rock bolting*, United States.

Sun, X. 1984. Grouted rock bolt used in underground engineering in soft surrounding rock or in highly stressed regions. *In: Proceedings of the International Symposium on Rock Bolting*, Balkema, Rotterdam.

Vlachopoulos, N., Carrapatoso, C., Holt, S,W., Cruz, D. and Forbes, B. 2020. An Investigation into Support Interaction of Ground Support through Numerical Modelling and Laboratory Testing, *Journal of Geotechnical and Geological Engineering*. Submission Number: GEGE-D-19-00935, accepted 26 April 2020.

Vlachopoulos, N., Cruz, D. and Forbes, B. 2018. Utilizing a novel fiber optic technology to capture the axial responses of fully grouted rock bolts, *Journal of Rock Mechanics and Geotechnical Engineering*, 10(2): 222-235.

Vlachopoulos, N. and Diederichs, M. 2014. Appropriate Uses and Practical Limitations of 2D Numerical Analysis of Tunnels and Tunnel Support Response. *Geotechnical and Geological Engineering*, 32(2): 469–488.

Vlachopoulos, N., Forbes, B. and Cruz, D. 2017. The Use of Distributed Optical Sensing Techniques for Ground Support; Not all Fiber Optic Methods are Similar. *In Proceedings of the 70th Annual Conference of the Canadian Geotechnical Society GeoOttawa*, Ottawa, Ontario, Canada.

Vlachopoulos, N., and Forbes, B. 2018. The Use of Distributed Fiber Optic Strain Sensing in Order to Conduct Quality Assurance and Quality Control for Ground Support. *In Proceedings of the 71st Annual Conference of the Canadian Geotechnical Society, GeoEdmonton,* Edmonton, Alberta, Canada.

Vlachopoulos, N., Forbes, B., Oke, J., and Hyett, A. 2014a. The Development of a Technique in order to Measure the Distributed Optical Sensing of a Forepole temporary support element employed within an Umbrella Arch System. *In ISRM Regional Symposium* - EUROCK, Vigo, Spain.

Vlachopoulos, N., Oke, J., and Forbes, B. 2014b. Determination of Mechanical Behaviour and Performance of Forepole Support Elements used in Tunnelling Forepoles. *In the Canadian Geotechnical Society's (CGS) 67th Canadian Geotechnical Conference*, Regina, Saskatchewan, Canada.

Windsor, C.R. 1997. Rock reinforcement systems, *International Journal of Rock Mechanics and Mining Sciences*, 34(6): 919-951.

Windsor, C.R. and Thompson, A.G. 1993. *Rock reinforcement—technology, testing, design and evaluation. In: Hudson JA (ed) Comprehensive rock engineering, principles, practice & projects*, 4nd ed., Oxford, London, UK.